Beneficial Effect of Nanoclay in Atom Transfer Radical Polymerization of Ethyl Acrylate: A One Pot Preparation of Tailor-Made Polymer Nanocomposite

Haimanti Datta, Nikhil K. Singha, and Anil K. Bhowmick*

Rubber Technology Centre, Indian Institute of Technology, Kharagpur, 721302, India

Received July 10, 2007; Revised Manuscript Received September 27, 2007

ABSTRACT: The atom transfer radical polymerization (ATRP) of ethyl acrylate (EA) was carried out in bulk at 90 °C in the presence of organically modified nanoclay as an additive. A remarkable enhancement in the rate of polymerization was observed and it was compared with the ATRP of EA without nanoclay. Time of dispersion of clay in monomer (t_d) prior to polymerization and the extent of clay loading were found to have a positive effect on polymerization rate. The polymerization proceeded through first-order kinetics and molecular weights increased linearly with conversion, close to the targeted molecular weights. The living nature of the end group was confirmed by MALDI-TOF-mass spectrometry and a chain extension experiment. Several factors may account for this unexpectedly rapid, yet controlled ATRP of EA in the presence of nanoclay additive. Fourier transform infrared spectroscopy (FTIR), nuclear magnetic resonance spectrometry (NMR), and dynamic mechanical thermal analysis (DMTA) studies showed that the added nanoclay interacts with the carbonyl group (>C═O) of the monomer and reduces the electron density in the conjugated C═C bond, thereby increasing the reactivity of the monomer. This particular interaction also has an effect in the dynamic equilibrium of activation−deactivation cycle in ATRP. Interestingly, the resulting nanocomposites had exfoliated clay particles, as evident from wide-angle X-ray diffraction (WAXD) and transmission electron microscopy (TEM) studies.

Introduction

The past few years have witnessed a rapid development in the field of controlled radical polymerization for synthesizing tailor-made polymers with well-defined architecture and predictable molecular weights.[1−5] A number of techniques have been explored to achieve this control: atom transfer radical polymerization (ATRP),[6,7] nitroxide mediated polymerization (NMP),[8] reversible addition fragmentation process (RAFT),[9,10] etc. to name a few. Among these, transition metal mediated ATRP appears to be the most versatile one because of its freedom on choice of monomers and tolerance over a wide range of functionality of monomers as well as solvents and initiating species. ATRP is based on a fast dynamic equilibrium established between the dormant species (alkyl halides or polymer chains with halogen atom at their end units) and active radicals. The transition metal complexes act as reversible halogen transfer agents which keep the active radical concentration very low ($\sim 10^{-8}-10^{-7}$ M) so as to avoid radical termination, resulting in controlled polymerization. Because of the very low concentration of active radicals, the rate of polymerization in any controlled radical polymerization is considerably slower than that of the conventional radical polymerization, especially on use of aromatic ligands as catalytic components.[1] Therefore, strategies must be developed that allow ATRP to be carried out for shorter time periods and with higher monomer conversions. Several groups have reported that polar solvents such as acetonitrile[11] or ethylene carbonate[12] or additives such as carboxylic acid[13] or phenol[14] can act as accelerators in ATRP. Even the beneficial effect of water has also been noticed.[15,16] A significant rate enhancement has been proposed by Wang and Armes[15] with unusually high monomer conversion (up to 99%) by the judicious choice of ∼50% of water in ATRP of methoxy capped oligo (ethylene glycol) methacrylate (OEGMA) at 20 °C. Haddleton et al.[13,14] proposed a rate enhancement effect on methylmethacrylate (MMA) by incorporation of phenol or carboxylic acids. Addition of phenol was reported to increase the apparent rate constant value by 358%.

A recent paper[17] explored the role of DNA molecules to enhance the polymer growth in a surface initiated polymerization of 2-hydroxyethyl methacrylate (HEMA) by ATRP. The accelerated effect was suspected to be a combined result of the highly charged sugar−phosphate backbones of the DNA molecules and formation of copper complexes with DNA bases.

As the literature survey indicates, the rate acceleration in ATRP by using suitable additives was primarily focused on the (meth)acrylate systems till date. Among the acrylate monomers, ethyl acrylate (EA) is an important constituent of acrylic elastomers. An extensive investigation on ATRP of ethyl acrylate has been reported earlier by the present authors.[18,19]

In this article, an in-depth comprehensive study shows that organically modified clay particles (nanoclay) as an additive has an accelerated effect on the ATRP of ethyl acrylate, using the CuBr/bpy catalyst system. Effect of dispersion time (of clay in monomer, prior to polymerization) and extent of clay loading have also been examined. The interesting role of nanoclay as an additive in ATRP is verified by controlled experiments and probable reasons are discussed. This investigation also shows that ATRP can be used to produce in situ polymer nanocomposites, which have created a surge of interest since the last two decades because of the significant improvement in many physical properties of the host matrix.[20,21] More recently, work is focused on to develop tailor-made polymer−clay nanocomposites that ensure and maintain the random dispersion of the single silicate layers and, simultaneously, provide more control over the polymer architecture, such as forming block copolymers and facilitating controlled functionalization. To name a few, notable contributions in this area come from Bottcher et al.[22]

* Corresponding author. E-mail: anilkb@rtc.iitkgp.ernet.in. Phone: +91-3222-283180. Fax: +91-3222-220312.

10.1021/ma071528s CCC: $40.75
Published on Web 12/12/2007

Table 1. Specification and Designation of Different Nanoclays[a]

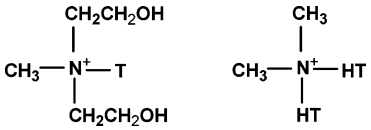

name	organic modifier
Cloisite 30B	MT2EtOT[b]
Cloisite 20A	2M2HT[c]
Cloisite NA+	−

[a] Surface area ~750 m^2/gm, layer thickness ~1 nm, aspect ratio ~50−200, initial particles consist of about 6000 platelets, dry particle size: 10% less than 2 μm, 50% less than 6 μm, and 90% less than 13 μm. [b] MT2EtOT: methyl, tallow (~65% C18; ~30% C16; ~5% C14, like oleic or linoleic acid), bis-2-hydroxyethyl, quaternary ammonium (structure shown above table, left). [c] 2M2HT: dimethyl, dihydrogenated tallow (~65% C18; ~30% C16; ~5% C14, like stearic acid), quaternary ammonium (structure shown above table, right).

and afterward Zhao et al.,[23] who reported the use of in situ ATRP by intercalating the initiator within silicate layers to produce polymer−clay nanocomposites. In addition, Jianbo and Sogah[24] described the one-step in situ block copolymerization involving simultaneous living free radical polymerization of styrene and anionic ring opening polymerization of ϵ-caprolactone in the presence of an initiator anchored montmorillonite (MMT). We have reported from our laboratory a series of publications[25−31] on the preparation and properties of various nanocomposites.

The aim of this work is (1) to investigate the role of nanoclay as an additive in the ATRP of ethyl acrylate and (2) to produce in situ polymer−clay nanocomposite where the polymer has sound controlled molecular weights and well-defined end group functionality.

Experimental Section

Materials. Ethyl acrylate (Aldrich, 99%) was washed twice with an aqueous solution of sodium hydroxide (5%) and twice with distilled water. The organic portion was dried with sodium carbonate (anhydrous) by overnight stirring, then filtered and finally distilled under reduced pressure over calcium hydride. The distillates were stored at −18 °C before they were used. CuBr (Aldrich, 98%) was stirred with glacial acetic acid for 12 h, washed with ethanol and diethyl ether, and then dried under vacuum at 75 °C for 3 days. The purified CuBr was stored in a nitrogen atmosphere. Methyl 2-bromopropionate (MBrP) (Alfa Aesar, 97%), 2,2′-bipyridine (bpy) (Lancaster, 98%), and all other chemicals were used as received. Nanoclays [Cloisite 30B, Cloisite NA+, and Cloisite 20A] were supplied by Southern Clay products, Gonzales, TX. Details of the nanoclays used in experiments are shown in Table 1.

General Polymerization Procedure. In a typical polymerization, the required amount of nanoclay was placed in a test tube (8 cm × 2.5 cm) provided with a B-14 standard joint and dispersed in monomer, ethyl acrylate (5 g, 4.9×10^{-2} mol) (already degassed by purging with nitrogen for 30 min before use), under a nitrogen atmosphere for different times at 25 °C. CuBr (0.0716 g, 4.9×10^{-4} mol) was added. It was then purged with nitrogen for 15 min. The ligand, 2,2′-bpy (0.1558 g, 9.8×10^{-4} mol), and finally the initiator, MBrP (0.0834 g, 4.9×10^{-4} mol), were added to the test tube in the sequential order via a dry and purified syringe at ambient temperature with continuous stirring. The reaction vessel was sealed with a rubber septum, which was secured by Cu wire, and was immersed into an oil bath maintained at a temperature of 90 °C and stirred. At different time intervals, the sample was withdrawn under a nitrogen atmosphere and a part of it was used for the gravimetric determination of monomer conversion. The rest was passed through a column of neutral alumina prior to size exclusion chromatography (SEC) analysis. After a specific time, the reaction was quenched by cooling the solution. The final polymer was passed through a column of neutral alumina oxide to remove the catalyst and then dried in a vacuum oven at 45 °C for 48 h.

Characterization. (a) Gel Permeation Chromatography (GPC). Molecular weights and molecular weight distributions of the polymer were determined by gel permeation chromatography (GPC) at ambient temperature using a Waters model 510 HPLC pump, a Waters series R-400 differential refractometer, and Waters Ultrastyragel columns of pore sizes 10 000, 1000, and 500 Å, which were preceded by a prefilter. THF was used as the eluent at a flow rate of 1.0 mL/min, and calibration was carried out using low polydispersity poly(methyl methacrylate) standards. Before injection into the GPC system, the polymer solutions were treated with cation exchange resin Dowex 50 W (Fluka) to make these free from Cu salts. For nanocomposite samples, the polymers were cleaved from clay by high-speed ultracentrifugation and filtration through a 0.2 μm filter.

(b) Fourier Transform Infrared Spectroscopy (FTIR). FTIR spectra were recorded using a Perkin-Elmer FTIR-spectrophotometer (model spectrum RX-I), within a range of 400−4400 cm^{-1} using a resolution of 4 cm^{-1}. An average of 16 scans has been reported for each sample. The samples were prepared by evaporating clay suspensions deposited on a KBr pellet in a vacuum desiccator under a pressure of 0.01 Torr.

(c) Nuclear Magnetic Resonance Spectrometry (NMR). ^{13}C NMR spectra were performed with a Bruker WM 300 spectrometer at 25 °C. ^{13}C NMR spectra were recorded in $CDCl_3$. It had a small amount of tetramethylsilane (TMS) added as an internal standard.

(d) Matrix-Assisted Laser Desorption Ionization Mass Spectrometry (MALDI-TOF-MS). MALDI-TOF-MS analyses were carried out using a Perceptive Biosystems Voyager Elite MALDI-TOF mass spectrometer, equipped with a nitrogen laser (wavelength 337 nm). For MALDI-TOF mass analysis, the matrix (2,5-dihydroxy benzoic acid) was dissolved in THF at a concentration of 40 mg/mL. Sodium trifluoroacetate was added to THF at a concentration of 1 mg/mL. The dissolved polymer concentration in THF was approximately 1 mg/mL. The matrix, salt, and polymer solutions were premixed in the ratio of 10/1/10. Approximately 0.5 μL of the obtained mixture was handspotted on the target plate to cover the 2.5 mm diameter sample position (typically 0.3 μL). The spot was allowed to air-dry without any assistance. Data were collected in linear as well as in reflectron mode, using delayed extraction, with a delay time of 350 ns. All the spectra were averaged over 128 laser shots.

(e) Dynamic Mechanical Thermal Analysis (DMTA). The mechanical properties of the polymers were measured using a dynamic mechanical analyzer (DMA) (Viscoanalyzer VA 4000 150N, Metravib). The samples were tested with an annular shear specimen holder, which allows to test the pasty sample and to follow in a single test evolution from the solid to pasty stage. The samples were heated from −50 to +50 °C at a heating rate of 2 °C/min at a constant frequency of 1 Hz, and the dynamic displacement was controlled by 5 μm. The loss tangent (tan δ) was measured as a function of temperature for all the samples under identical conditions.

(f) Wide-Angle X-ray Scattering (WAXS). The X-ray diffraction analysis was performed using a Rigaku Dmax 2500 diffractometer with a Co target ($\lambda = 0.179$ nm) at room temperature. The system consisted of a rotating anode generator, operated at 40 kV and 30 mA current and a wide angle goniometer. The samples were scanned from $2\theta = 2°$ to 10° at the step scan mode (step size 0.03°, preset time 2 s), and the diffraction pattern was recorded using a scintillation counter detector.

(g) Transmission Electron Microscopy (TEM). The distribution of clay particles into the polymer matrix was studied using a HR TEM (JEOL 2000) operated at an accelerated voltage of 200 kV. The samples were sectioned into ~100 nm thin sections at −50 °C using an ultra-cryomicrotome (Ultracut R, Leica) equipped with a glass knife. These cryotomed sections were then transferred to the copper grid and were observed through the microscope.

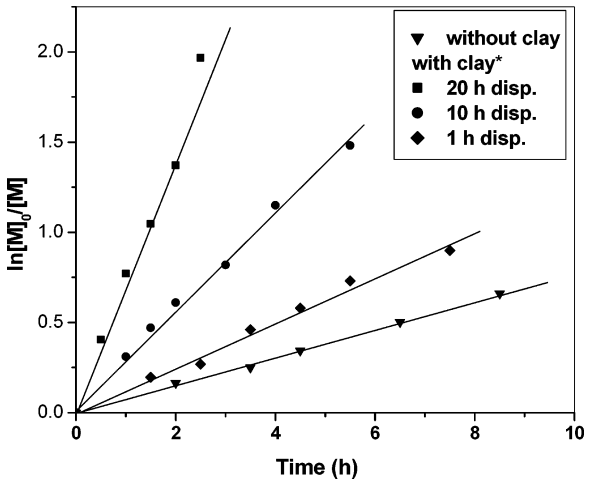

Figure 1. Semilogarithmic kinetic plots for the ATRP of EA in bulk at 90 °C. $[EA]_o = 4.9 \times 10^{-2}$ M, $[MBrP]_o = 4.9 \times 10^{-4}$ M, $[CuBr] = 4.9 \times 10^{-4}$ M, $[bpy] = 9.8 \times 10^{-4}$ M. *Nanoclay used: Cloisite 30B (2 wt %).

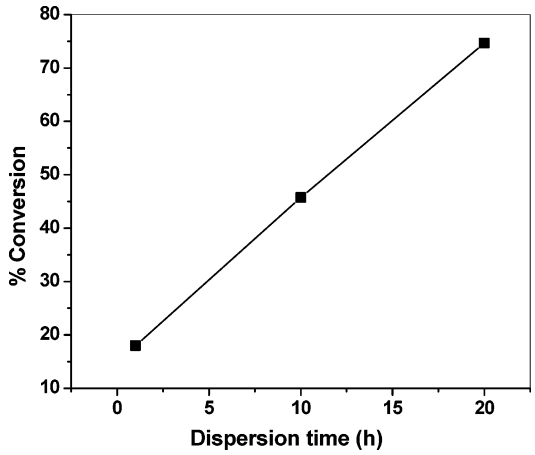

Figure 2. Effect of dispersion time of the clay in monomer (prior to polymerization) on % conversion in ATRP of EA in bulk at 90 °C at 2 h. $[EA]_o = 4.9 \times 10^{-2}$ M, $[MBrP]_o = 4.9 \times 10^{-4}$ M, $[CuBr] = 4.9 \times 10^{-4}$ M, $[bpy] = 9.8 \times 10^{-4}$ M.

Results and Discussion

Effects of Nanoclay as Additive in ATRP of EA. EA was polymerized in bulk using MBrP as an initiator, CuBr as a catalyst, bpy as a ligand, and nanoclay (Cloisite 30B) as an additive at 90 °C. Figure 1 shows the kinetic plots of the ATRP systems at different dispersion times (t_d) of the clay in the monomer prior to polymerization. It indicates that in all the cases ln $[M]_o/[M]$ increases linearly with increasing reaction time t, demonstrating that the active radical concentration remains constant during polymerization. Also, the side reactions like irreversible chain transfer or chain termination are quite limited.[1] Importantly, Figure 1 also reveals that there is a noteworthy effect of t_d on the kinetics of polymerization. With increasing t_d, the polymerization rate increases; this subsequently leads to higher fractional conversion (of monomer) after a specific time period, as registered in Figure 2.

Addition of 2 wt % of nanoclay dramatically increases the polymerization rate, reaching 77% conversion in 5.5 h (at t_d = 10 h) in contrast to the control experiment (without clay) where 58% conversion has been achieved in 10.5 h. This remarkable increase in polymerization rate is observed from an increase in the gradient, the apparent rate constant (k_{app}) of polymerization. The k_{app} value increases by 62% for 1 h of dispersion, 247% for 10 h, and 866% for 20 h (Table 2).

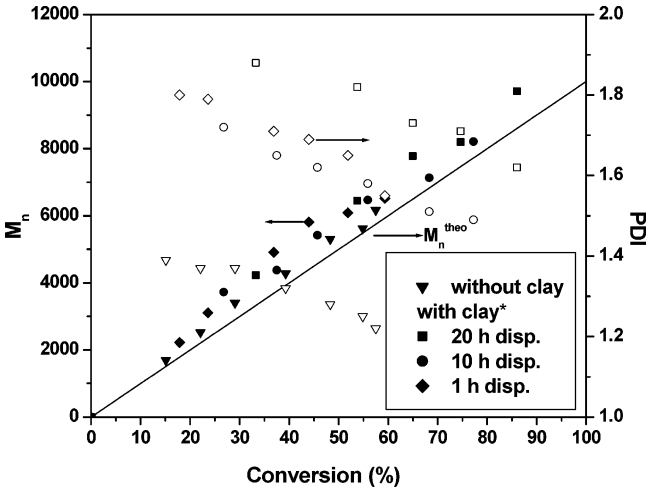

Figure 3. Plots of M_n^{SEC} and PDI versus monomer conversion for in situ ATRP of EA-clay* nanocomposite at 90 °C with varying dispersion time. $[EA]_o = 4.9 \times 10^{-2}$ M. Open symbols represent polydispersities and filled symbols represent M_n^{SEC}. *Nanoclay used: Cloisite 30B (2 wt %).

Table 2. Variation of k_{app} as a Function of Dispersion Time (of Clay[a] in Monomer) in ATRP of EA in Bulk at 90 °C

dispersion time (t_d)	sample designation (of clay in monomer)	sample designation (of resultant polymer)	k_{app} (s^{-1}), $\times 10^{-5}$	% increase
without clay			2.14	
1 h	EAD 1	PEAD 1	3.47	62
10 h	EAD 10	PEAD 10	7.43	247
20 h	EAD 20	PEAD 20	20.68	866

[a] Nanoclay used: Cloisite 30B, 2 wt %.

With increasing swelling time, more monomer penetrates the organophilic interlayer region and thus the concentration of EA inside the gallery spacing increases tremendously (as evidenced by the enhancement in *d*-spacing, by WAXD analysis; not shown here). This facilitates the rate of polymerization. Similar kind of observations has been reported in the literature[32] that when the clay shows good compatibility or interaction with monomer, a significant swelling of the clay galleries by the monomer is obtained. The proposed mechanism is discussed later.

Figure 3 shows the GPC results of the resultant polymer samples taken at different time intervals and monomer conversions. Molecular weights (M_n) increase linearly with conversion along with a regular decrease in polydispersity indices (M_w/M_n), which confirms the living nature of polymerization. M_n values determined by GPC (M_n^{exptl}) show a good agreement with theoretical ($M_n^{theoret}$) values. These results are in contrast to the previously reported[23] in situ nanocomposite system based on polystyrene and poly(methyl methacrylate), where the polymers showed a significant deviation between $M_n^{theoret}$ and M_n^{exptl}. The earlier authors, however, adopted a different approach, viz., by intercalating ATRP initiator in between silicate layers followed by polymerization, to prepare an in situ nanocomposite and did not report any rate-accelerating effect of nanoclay on the ATRP of acrylates. The polydispersity index (PDI) is a little broader; the lowest molecular weight distribution is achieved in the polymer PEAD10 (1.49), where clay (Cloisite 30B) has been dispersed for 10 h in monomer prior to polymerization. A very fast polymerization rate in the case of PEAD20 renders loss of control over polymerization and the

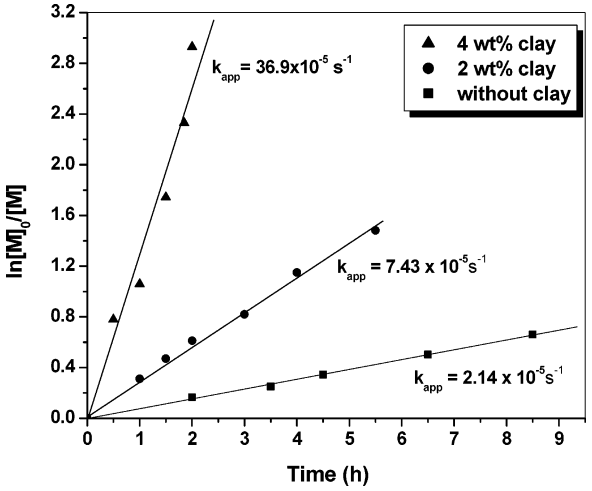

Figure 4. Effect of clay* loading on reaction kinetics of ATRP of EA at 90 °C. $[EA]_o = 4.9 \times 10^{-2}$ M, $[MBrP]_o = 4.9 \times 10^{-4}$ M, $[CuBr] = 4.9 \times 10^{-4}$ M, [bpy] = 9.8×10^{-4} M. *Nanoclay used: Cloisite 30B.

possibility of side reactions leads to PDI values quite broader (1.62).

Clay loading also has a catalyzing effect on the polymerization rate (Figure 4), reactions being carried out at t_d =10 h. The apparent rate constant value (k_{app}) increases from 2.14×10^{-5} s^{-1} in the absence of clay to 7.43×10^{-5} s^{-1} for 2 wt % clay loading and to 36.9×10^{-5} s^{-1} where clay loading is 4 wt %. For clay content more than 4 wt %, the reaction medium became very viscous soon and hence the kinetic study could not be carried out.

The kinetics and GPC results indicate that addition of nanoclay (Cloisite 30B) as an additive in ATRP of EA lead to an appreciably high polymerization rate but still preserve the basic criteria of a well-controlled ATRP system to a large extent. In-depth research was carried out to understand the underlying reaction mechanism.

Nanoclays used in the present study belong to the general family of 2:1 layered phyllosilicates. Their crystal structure consists of layers made up of two tetrahedrally coordinated silicon atoms fused to an edge shared octahedral sheet of Al-$(OH)_3$. Stacking of the layers leads to a regular van der Waals gap called the interlayer or gallery. In nanoclays, clay surfaces are rendered organophilic on substitution of alkali or alkaline earth cations situated inside this interlayer spacing by long chain alkyl ammonium ions, resulting in a larger gallery spacing (e.g., 1.85 nm in Cloisite 30B, compared to 1.17 nm in unmodified clay, Cloisite NA+).

The lyotropic series[33] (for ion exchange of clay) indicates that the transition metals like Cu^+ are not a good exchangeable cation for NH_4^+, attached to the organic surfactant moiety, unless some special conditions are maintained (for example, lowering in surface potential, etc., by using some external agents). Hence, it might be argued that during polymerization, there is very less probability of the cation exchange phenomena (Cu^+ for NH_4^+) to take place. This consequently prevents the release of surfactants and thereby modification of the coordination of Cu^+ in polymerization.

The acceleration effects from the use of polar solvents or polar additives, especially using those having an active hydroxyl group, e.g., phenol, carboxylic acid, water, etc., in ATRP have been reported previously.[11−16,34,35] It has been reported that an improvement in radical activation rate and a decrease in the radical recombination rate collectively lead to the observed

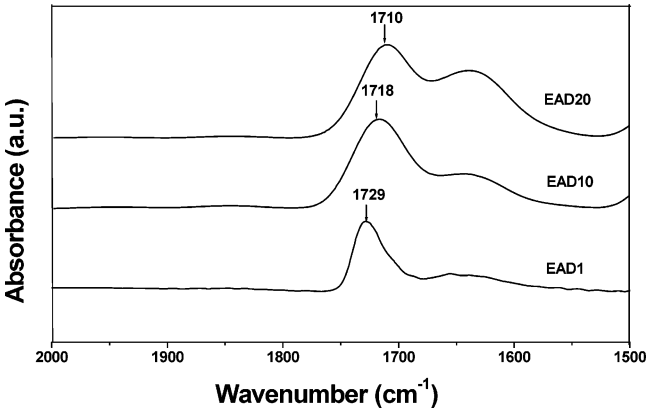

Figure 5. FTIR spectra of EA at different dispersion times.

phenomena in those cases. Matyjaszewski et al.[12,36] proposed the generation of the more reactive $[Cu^I(bpy)_2]^+$ complex with a halide counterion as the intermediate species in a polar medium in contrast to the neutral binuclear complex, formed in conventional ATRP. Furthermore, a recent report[37] has shown that a negatively charged surface could concentrate positively charged catalysts (i.e., Cu ions) and subsequently enhance the chain growth rate. A similar mechanism can be postulated in our case also, where clay provides the negative charge surface and the active hydroxyl group (present in the surface as well as in the modifier) imparts polar character in the reaction medium, thereby encouraging the generation of active ionic intermediate species.

In order to understand the effect of hydroxyl groups on ATRP of EA, the polymerization was carried out in the presence of isopropanol (2 wt %) as an additive. In this case, only a marginal improvement in the polymerization rate is observed (62% conversion in 10.5 h) compared to that in conventional ATRP (58% conversion in 10.5 h). A similar effect was observed when the role of "excess" surfactant (MT2EtOT) present in commercially available clay (Cloisite 30B) was analyzed by cleaving it from clay by extraction in toluene, followed by removal of solvent. We carried out the polymerization at 90 °C in bulk in the presence of the cleaved surfactant (released from 2 wt % of clay), at similar polymerization conditions used in presence of 2 wt % of clay. A marginal improvement in the polymerization rate (61% conversion in 10.5 h) is observed in this case, compared to the neat polymer (in the absence of nanoclay), but much lesser than that obtained in the presence of nanoclay.

This is attributed to the presence of the polar hydroxyl groups (in modifier), which incorporates polarity to the reaction medium and thereby accelerates the polymerization rate to some extent.

Hence, it is obvious that this high degree of acceleration effect in the present case is not exclusively due to the polar nature of the medium and a different mechanism must also be in effect during the polymerization. In order to elucidate the impact of the nanoclay, we explored this further by FTIR.

Figure 5 shows the FTIR spectra for the carbonyl absorption of EA in the presence of nanoclay at different dispersion times (t_d). Interestingly, it is observed that with increasing t_d, the band position of >C═O stretching is shifted (by 11 cm^{-1} in the case of EAD10 and 19 cm^{-1} in EAD20) toward lower frequency. Concomitantly, a definite change in clay structure is also noticed; the peak at 3635 cm^{-1}, attributed to the stretching frequency of the structural hydroxyl group (from >Al−O−H),[38] is shifted to lower wavenumber values (Figure 6). It indicates that the >Al−O−H group of the clay layers interacts with the >C═O group of the acrylate monomer. This particular interaction

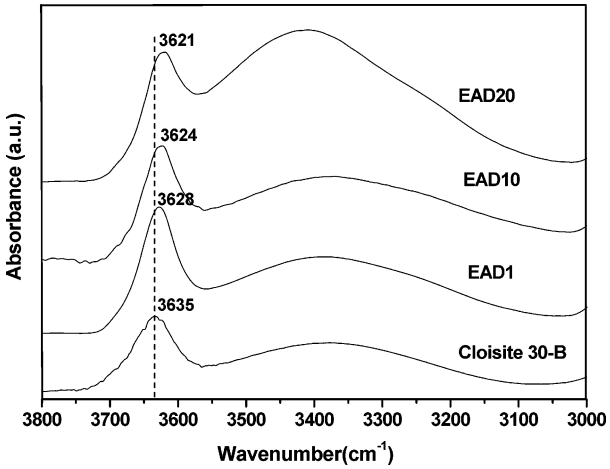

Figure 6. Change in clay structure at different dispersion times.

Scheme 1. Schematic Representation of Coordination of Clay with Monomer

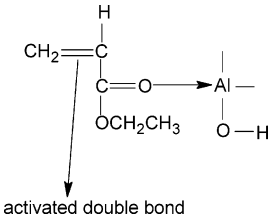

($>C^{\delta-}=O^{\delta+}\cdots^{\delta-}Al-O-H$) tends to decrease the double bond character of the carbonyl group, therefore shifting the absorption band to lower frequency. Participation of Al on polymerization is also established by the lowering of the Al−O stretching frequency value from 477 cm^{-1} (in nanoclay) to 463 cm^{-1} in the resulting hybrid material (Supporting Information, Figure S2).

Coordination of the nanoclay with the carbonyl group of the acrylate moiety is further corroborated by ^{13}C NMR spectra shown in Figure 7 a,b. On addition of nanoclay, the resonance due to carbonyl absorption exhibits a lower chemical shift, hence, supporting the proposed mechanism, i.e., there is a definite coordination of the carbonyl group of the acrylate moiety to the electron deficient Al-atom in the nanoclay. Very recently, Luo and Sen[39] reported a notable enhancement of the polymerization rate in acrylates in the nitroxide mediated as well as RAFT mediated controlled radical polymerization using solid acidic alumina (Al_2O_3) as an additive. They explained this interesting observation by the coordination of >C═O group in the acrylate moiety with Al_2O_3, which acts as a Lewis acid.

From the FTIR and ^{13}C NMR studies and the recent investigations, it is clearly understood that the electron deficient Al in nanoclay coordinates with the >C═O group of the acrylate monomer (shown in Scheme 1) and reduces the electron density in the conjugated C═C bond, thereby increasing the reactivity of the monomer.

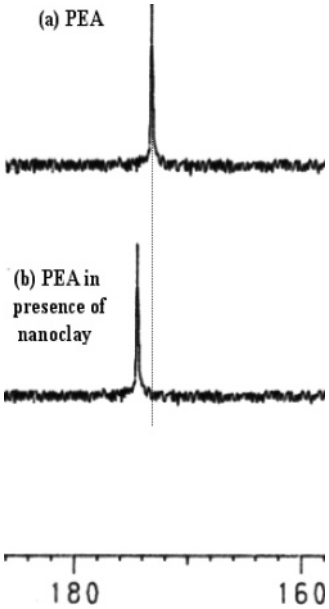

Figure 7. ^{13}C NMR spectra of poly(ethyl acrylate) in the presence and absence of nanoclay at 25 °C.

This interaction of >C═O with the Al in the nanoclay has an interesting effect in the dynamic equilibrium of the activation−deactivation cycle in ATRP (Scheme 2). The >Al−O−H group of the nanoclay interacts with the >C═O group of the dormant species (PEA-Br); thereby activating the C−Br bond next to the ester carbonyl bond.

This results in increasing the rate of initiation and propagation, thereby enhancing the rate of polymerization. With increasing dispersion time, more EA molecules penetrate the intergallery spacing in the nanoclay, thus encouraging more interaction between the >C═O group and the Al atom in the nanoclay and hence promotes the polymerization rate. FTIR also shows that there is a gradual shift of >C═O stretching frequency with increasing dispersion time (t_d). Moreover, from the thermodynamic point of view, the apparent propagation activation enthalpy in ATRP is composed of the radical propagation activation enthalpy and activation enthalpy of the halogen transfer. Coordination of the >C═O group may lower the activation enthalpy of the halogen atom transfer and consequently reduces the apparent propagation activation enthalpy.[36] This subsequently increases the dynamic equilibrium constant between radicals and the dormant species, thereby encouraging the generation of active radicals in the medium and the polymerization rate gets enhanced. In a controlled experiment, styrene, a noncoordinating monomer was polymerized via ATRP using nanoclay as the additive (Supporting Information, Table-S1). Interestingly, in this case there was no significant improvement in the polymerization rate as compared to the system devoid of nanoclay. This subsequently confirms the participation of the >C═O group in the monomer EA with the nanoclay. Guo et al.[40] reported ATRP of methacrylate monomers (butyl

Scheme 2. Proposed Mechanism of Redox Dynamic Equilibrium in Presence of Nanoclay as an Additive

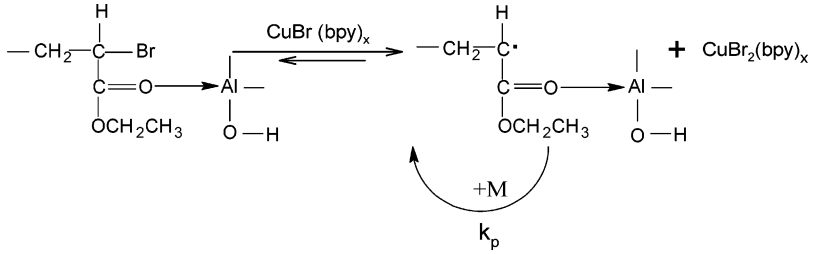

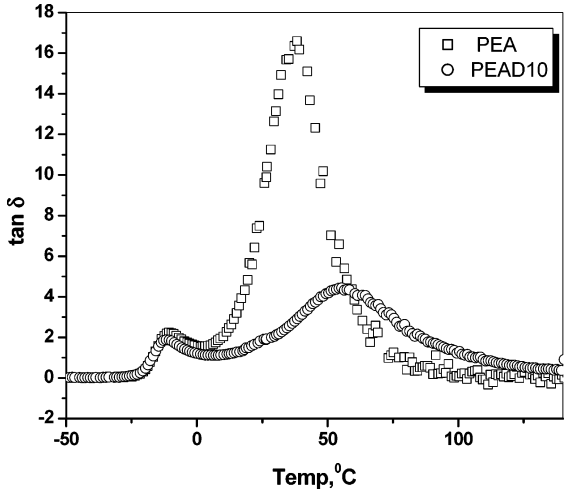

Figure 8. tan δ vs temperature plot of neat polymer and in situ prepared hybrid composite.

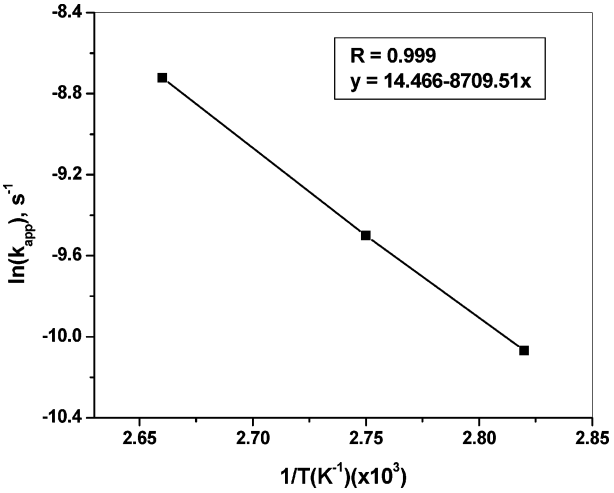

Figure 9. Plot of ln k_{app} versus $1/T$ for ATRP of EA in the presence of nanoclay initiated by MBrP with CuBr/bpy as the ligand in bulk. [EA]/[MBrP]/[CuBr]/[bpy] = 100/1/1/2.

methacrylate, methyl methacrylate) promoted by aluminum isopropoxide. The enhanced rate of polymerization was explained in terms of coordination between the >C═O group of the monomer to aluminum propoxide, a Lewis acid.

The above-proposed mechanism is again established by dynamic mechanical analysis of the neat polymer and its hybrid composite. Figure 8 represents the temperature dependence of tan δ for the virgin polymer and the in situ prepared composite sample (PEAD10) at 2 wt % clay loading. tan δ, the ratio of the loss modulus to the storage modulus, is related to the molecular mobility transition such as glass transition temperature (T_g). The figure shows two different transitions in each sample; the lower temperature peak may be termed as the α-transition temperature (T_α), which arises from the relaxation of the main backbone chain. It corresponds to the glass transition temperature (T_g) of the polymer matrix. The secondary transition may be termed as the liquid−liquid-transition temperature (T_{ll}), which is attributed to the shifting of the entire molecule by cooperative segmental motion.[41] Unlike T_α, the T_{ll} values were not much affected in the presence of clay.

In the present case, because of the short chain length of the polymer (targeted degree of polymerization = 100), restriction of the segmental Brownian motion of the polymer chains is not affected much in the nanocomposites. It is interesting to note that there is a significant effect of clay tactoids on the T_{ll} transition; a positive shift of transition temperature by 17 °C is observed for hybrid composite material along with a dramatic decrease in the tan δ peak height compared to the pristine polymer. Literature reports that the intensity of this transition becomes prominent in low-molecular weight polymers, with narrowing molecular weight distributions.[42] In the present case, the polymers fulfill both the criterions. With the tool of ATRP, the polymer is prepared with well-defined molecular weights and narrow molecular weight distributions.[1] The incorporation of nanoclay, as the mechanism proposes, develops an interaction with the side-chain acrylate unit. The presence of this interaction severely restricts the movement of the entire molecule (much more than it would restrict mere segmental motion), and a higher temperature is required for the same transition to occur, leading to a suppression of the tan δ peak height as well. The values of T_g and T_{ll} of polyethyl acrylate are reported in the literature,[43] supporting the discussion mentioned above.

The importance of interaction between the nanoclay and the monomer was further substantiated by taking clays of various gallery heights, viz., Cloisite NA^+, i.e., unmodified clay and Cloisite 20A, in addition to Cloisite 30B (Table 3). It is postulated that due to the organophilic nature of clay, monomer molecules penetrate into the interlayer region where polymerization occurs. The polymerizations were carried out at t_d = 10 h. From the results of Table 3, it is observed that the conversion increases with increasing gallery spacing. In addition, the enhanced compatibility of the nanoclay (Cloisite 30B and Cloisite 20A) with monomer compared to that of the unmodified clay (Cloisite NA) is another factor which might be accountable for this particular observation. It may be proposed that an increase of gallery spacing as well as compatibility of monomer with clay facilitates intercalation of more monomers, which then interact with the clay, thereby enhancing the polymerization rate.

Table 3. Effect of Types of Nanoclay in Kinetics of ATRP of EA at 90 °C

type of clay	interlayer spacing (nm)	% conversion at 5.5 h	apparent rate constant of polymerization, k_{app}, s^{-1} ($\times 10^{-5}$)
Cloisite NA+	1.17	69	5.91
Cloisite 30B	1.85	77	7.43
Cloisite 20A	2.42	81	7.90

ATRP of EA was examined at three different temperatures, viz., 80 °C, 90 °C, and 100 °C to calculate the activation energy of polymerization. Reaction temperature registers a positive effect on polymerization kinetics and their corresponding apparent rate constant (k_{app}) value has been calculated. The Arrhenius plot of ln (k_{app}) versus $1/T$ obtained from the experimental results is given in Figure 9. On the basis of the slope of the plot, an apparent enthalpy of activation ($\Delta E^{\ddagger}_{app}$) of 72.4 kJ/mol is determined, which is quite lower than the corresponding value (84.7 kJ/mol) for the monomer,[19] without using any additive attributing to higher rate of polymerization.

Morphology Study of in Situ Prepared Nanocomposites by WAXD and TEM. Effect of dispersion time on polymerization was further supported by the wide-angle X-ray diffraction (WAXD) study. Figure 10 shows the WAXD patterns of the nanoclay, neat polymer, and PEA−clay composites at different dispersion times. At lower dispersion time (t_d = 1 h), the resultant polymer (PEAD1) shows some agglomeration of clay particles as indicated by retention of the layered structure to a certain extent. Efficient penetration of the polymer chains in between the clay galleries is observed with increasing t_d, where no discernible peak due to clay is present, delineating a

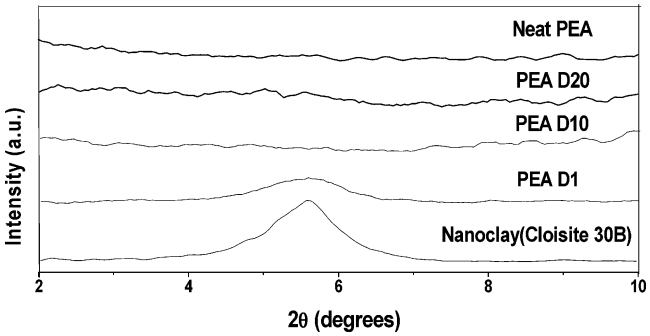

Figure 10. XRD patterns of PEA−clay hybrid composites at different dispersion times.

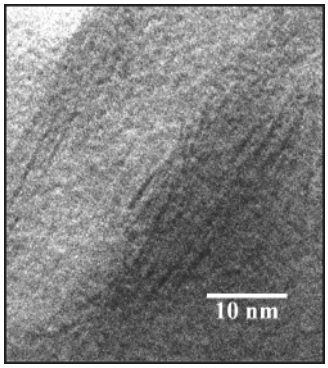

Figure 11. TEM micrograph of PEA−clay nanocomposite PEAD10.

significant disruption in the hierarchical layered structure. In PEAD10 and PEAD20, a complete absence of peaks in between $2\theta = 2-10°$ indicates that the systems are totally exfoliated. It has been reported earlier from our group that the exfoliation/intercalation is a function of the structure of polymer and nanoclay in the case of rubbery polymers.[25,28] Similarly, it can be argued that in this case also polar−polar interactions of the matrix with the nanoclay may be the prime factor. The polar polymer matrix interacts with the clay surface and registers a good matrix−filler interaction. Another parameter is the controlled nature of polymerization where the targeted degree of polymerization was designed to be low (100). This facilitates the penetration of short chain polymers within clay galleries and hence promotes a large degree of exfoliation.

To substantiate the X-ray results, a TEM study of the sample PEAD10 was undertaken and the respective micrograph is demonstrated in Figure 11. The clay layers appear as dark strips but the polymer matrix as a gray/white domain. The lamellar nanocomposite showed a mixed morphology. Individual silicate layers, along with two, three, and four layer stacks, are exfoliated in the PEA matrix. In addition, some larger intercalated tactoids could also be identified. The results are in good agreement with XRD data where no basal (001) reflection was observed.

End Group Analysis. End group analysis of polymers[44] prepared by ATRP is important because polymer chains with halogen end groups act as a macroinitiator. It can be reactivated in the presence of the ATRP catalytic system to initiate the polymerization of the second monomer to form a block,[6] graft,[45] or star polymer, etc., depending on the position and numbers of initiation sites. The chain end functionalities were analyzed by matrix-assisted laser desorption ionization time-of-flight mass spectrometry (MALDI-TOF-MS).

Figure 12 displays a selected part of the MALDI-TOF mass spectrum of ethyl acrylate prepared by using MBrP as the initiator and the CuBr/bpy catalytic system. This shows an envelope of species each separated by approximately 100 mass

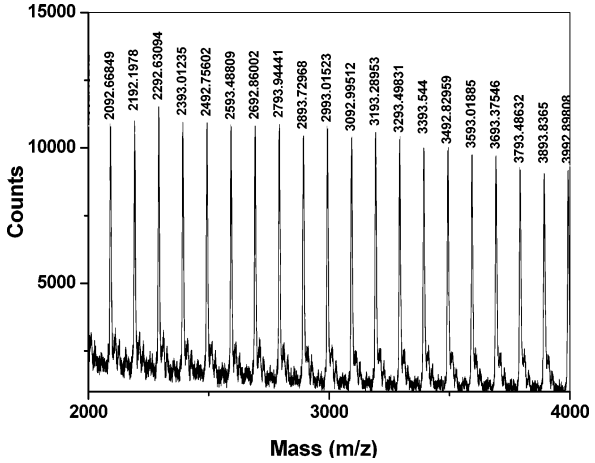

Figure 12. MALDI-TOF mass spectrum of poly(ethyl acrylate)−clay nanocomposite synthesized by ATRP.

units, the molar mass of the repeat unit of EA. On the basis of molecular weight values and the isotope distribution, the signals of each major peak correspond to structure-I.

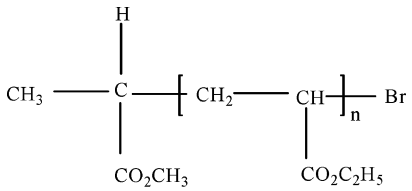

Structure-I

For example, the peak at *m*/*z* 2292 can be assigned to structure-I, where $n = 21$ and Na salt is the cationic agent.

Adding a fresh aliquot of monomer in a chain extension experiment also evidences retention of the "living" nature of the polymer in the presence of nanoclay. Thus, the isolated PEA is further used as a macroinitiator to initiate the polymerization of fresh EA at 90 °C in the bulk using CuBr as a catalyst and bpy as a ligand. A block copolymer is produced, as is evident from the GPC traces (Supporting Information, Figure S1). The shift of the block copolymer trace toward higher molecular weight along with lowering of the PDI shows the efficient initiation by the PEA macroinitiator. It clearly indicates the controlled nature of nanoclay-enhanced polymerization of EA as well as its "living characteristics".

Conclusions

Use of nanoclay as an additive in ATRP of EA leads to a tremendous increase in the polymerization rate as observed from the increase in the gradient, the apparent rate constant (k_{app}) of polymerization. The k_{app} value increased by 62% for 1 h dispersion, 247% for 10 h, and 866% for 20 h. Dispersion time of the clay in the monomer prior to polymerization and the extent of clay loading are found to have a positive effect on the kinetics of polymerization. The resultant polymers have controlled molecular weights and well-defined end groups. FTIR, NMR, and DMTA studies demonstrate that there is a definite interaction between the hydroxyl groups of the clay with that of the carbonyl moiety of the dormant species, thereby activating the C−Br bond next to the ester carbonyl bond generating a higher concentration of active radicals. On the basis of the slope of the Arrhenius plot, an apparent enthalpy of activation ($\Delta E^{\ddagger}_{app}$) of 72.4 kJ/mol is determined. The structure of resulting nanocomposites appears to be mostly exfoliated as examined by WAXD and TEM. Retention of the living end group in

polymer−clay nanocomposite has been confirmed by MALDI-TOF-mass spectrometry as well as the chain extension experiment. Interestingly, this in situ ATRP of EA using nanoclay as an additive leads to tailor-made PEA nanocomposites.

Supporting Information Available: ATRP of styrene (St) in bulk at 90 °C, GPC traces of PEA-Br macroinitiator and PEA-*b*-PEA diblock copolymers synthesized by chain extension reaction, and FTIR spectra of neat clay and its hybrid composite at $t_d = 10$ h. This material is available free of charge via the Internet at http://pubs.acs.org.

References and Notes

(1) Matyjaszewski, K. Ed. *Controlled Radical Polymerization*; ACS Symposium Series 685; American Chemical Society: Washington, DC, 1997.
(2) Otsu, T.; Matsumoto, A. *Adv. Polym. Sci.* **1998**, *136*, 75.
(3) Fukuda, T.; Goto, A.; Ohno, K. *Macromol. Rapid Commun.* **2000**, *21*, 151.
(4) Sawamoto, M.; Kamigaito, M. *Polymer Synthesis*; Materials Science and Technology Series; VCH-Wiley: Weinheim, Germany, 1998.
(5) Georges, M. K.; Veregin, R. P. N.; Kazmaier, P. M.; Hamer, G. K. *Trends Polym. Sci.* **1994**, *2*, 66.
(6) Wang, J. S.; Matyjaszewski, K. *J. Am. Chem. Soc* **1995**, *117*, 5614.
(7) Kato, M.; Kamigaito, M.; Sawamoto, M.; Higashimura, T. *Macromolecules* **1995**, *28*, 1721.
(8) Georges, M. K.; Moffat, K. A.; Veregin, R. P. N.; Kazmaier, P. M.; Hamer, J. K. *Polym. Mater. Sci. Eng.* **1993**, *69*, 305.
(9) Le, T. P. T.; Moad, G.; Rizzardo, E.; Thang, S. H.; Du Pont. PCT Int. Appl. WO 9801478, 1998.
(10) Chiefari, J.; Chong, Y. K.; Ercole, F.; Krstina, J.; Jeffery, J.; Le, T. P. T.; Mayadunne R. T. A.; Meijs, G. F.; Moad, C. L.; Moad, G.; Rizzardo, E.; Thang, S. H. *Macromolecules* **1998**, *31*, 5559.
(11) Wang, X. S.; Luo, N.; Ying, S. K. *J. Polym. Sci., Part A: Polym. Chem.* **1999**, *37*, 1255.
(12) Matyjaszewski, K.; Nakagawa, Y.; Jasieczek, C. B. *Macromolecules* **1998**, *31*, 1535.
(13) Haddleton D. M.; Heming, A. M.; Kukulji, D.; Duncalf, D. J.; Shooter, A. J. *Macromolecules* **1998**, *31*, 2016.
(14) Haddleton, D. M.; Clark, A. J.; Crossman, M. C.; Duncalf, D. J.; Hemimg, A. M.; Morsely, S. R.; Shooter, A. *J. Chem. Commun.* **1997**, 1173.
(15) Wang, X. S.; Armes, S. P. *Macromolecules* **2000**, *33*, 6640.
(16) Chatterjee, U.; Jewrajka, S. K.; Mandal, B. M. *Polymer* **2005**, *46*, 1575.
(17) Lou, X.; He, L. *Langmuir* **2006**, *22*, 2640.
(18) Datta, H.; Bhowmick, A. K.; Singha, N. K. *Macromol. Symp*. **2006**, *240*, 245.
(19) Datta, H.; Bhowmick, A. K.; Singha, N. K. *J. Polym. Sci., Part A: Polym. Chem.* **2007**, *45*, 1661.
(20) Ray, S. S.; Okamoto, M. *Prog. Polym. Sci.* **2003**, *28*, 1539.
(21) (a) Giannelis, E. P. *Adv. Mater*. **1996**, *8*, 29. (b) Wong, S.; Vaia, R.; Vasudevan, S.; Giannelis, E. P.; Zax, D. B. *J. Am. Chem. Soc*. **1995**, *117*, 7568. (c) Vaia, R. A.; Vasudevan, S.; Karwiec, W.; Scanlon, L. G.; Giannelis, E. P. *Adv. Mater*. **1995**, *7*, 154. (d) Krishnamoorti, R.; Vaia, R. A.; Giannelis, E. P. *Chem. Mater*. **1996**, *8*, 1728. (e) Giannelis, E. P.; Krishnamoorti, R.; Manias, E. *Adv. Polym. Sci.* **1999**,*138*, 107.
(22) Bottcher, H.; Hallensleben, M. L.; Nuss, S.; Wurm, H.; Bauer, J.; Behrens, P. *J. Mater. Chem.* **2002**, *12*, 1351.
(23) Zhao, H.; Argoti, D. S.; Farrel, B. P.; Shipp, D. A. *J. Polym. Sci., Part A: Polym. Chem.* **2004**, *42*, 916.
(24) Jianbo, D.; Sogah, D. S. *Macromolecules* **2006**, *39*, 5052.
(25) Maiti, M.; Bhowmick, A. K. *J. Polym. Sci., Part B: Polym. Phys.* **2006**, *44*, 162.
(26) Patel, S.; Bandyopadhyay, A.; Ganguly A.; Bhowmick, A. K. *J. Adhes. Sci. Technol.* **2006**, *20*, 371.
(27) Bandopadhyay, A.; Sarkar, M. De.; Bhowmick, A. K. *Rubber Chem. Technol*. **2005**, *78*, 806.
(28) Sadhu, S.; Bhowmick, A. K. *J. Polym. Sci., Part B: Polym. Phys.* **2004**, *42*, 1573.
(29) Sadhu, S.; Bhowmick, A. K. *J. Mater. Sci.* **2005**, *40*, 1633.
(30) Sadhu, S.; Bhowmick, A. K. *J. Polym. Sci., Part B: Polym. Phys.* **2005**, *43*, 1854.
(31) Ganguly, A.; Sarkar, M. De. *J. Polym. Sci., Part B: Polym. Phys.* **2007**, *45*, 52.
(32) Pluart, L.; Duchet, J.; Sautereau, H.; Halley, P.; Gerard, J.-F. *Appl. Clay Sci.* **2004**, *25*, 207.
(33) Worrall, W. E. *Clays: Their Nature, Origin and General Properties*; Maclaren & Sons: London, U.K., 1968; p 50.
(34) Bontempo, D.; Tirelli, N.; Masci, G.; Crescenzi, V.; Hubbell, J. A. *Macromol. Rapid Commun.* **2002**, *23*, 418.
(35) Narain, R.; Armes, S. P. *Biomacromolecules* **2003**, *4*, 1746.
(36) Matyjaszewski, K.; Patten, T. E.; Xia, J. H. *J. Am. Chem. Soc*. **1997**, *119*, 674.
(37) Kizhakkedathu, J. N.; Brooks, D. E. *Macromolecules* **2003**, *36*, 591.
(38) Wada, K. *Clay Miner*. **1967**, *7*, 51.
(39) Luo, R.; Sen, A. *Macromolecules* **2007**, *40*, 154.
(40) Guo, J.; Han, Z.; Wu, P. *J. Mol. Catal., Part A: Chem*. **2000**, *159*, 77.
(41) (a) Boyer, R. F. *J. Polym. Sci., Part C* **1966**, *14*, 267. (b) Boyer, R. F. *Rubber Chem. Technol.* **1963**, *36*, 1303.
(42) Glandt, C. A.; Toh, H. K.; Gillham, J. K.; Boyer, R. F. *J. Appl. Polym. Sci.* **1976**, *20*, 1277.
(43) Kumler, P. L.; Machajewski, G. A.; Fitzgerald, J. J.; Denny, L. R.; Keinath, S. E.; Boyer, R. F. *Macromolecules* **1987**, *20*, 1060.
(44) Gaynor, S. G.; Matyjaszewski, K. *ACS Symp. Ser*. **2000**, *768*, 347.
(45) Roos, S. G.; Mueller, A. H. E.; Matyjaszewski, K. *Macromolecules* **1999**, *32*, 8331.

MA071528S